

PAPER

## Flux creep after field trapping in $\text{YBa}_2\text{Cu}_3\text{O}_x$ foams

To cite this article: M R Koblischka *et al* 2020 *Supercond. Sci. Technol.* **33** 044008

View the [article online](#) for updates and enhancements.



**IOP | ebooks™**

Bringing together innovative digital publishing with leading authors from the global scientific community.

Start exploring the collection—download the first chapter of every title for free.

# Flux creep after field trapping in $\text{YBa}_2\text{Cu}_3\text{O}_x$ foams

M R Koblischka<sup>1,3</sup> , S Pavan Kumar Naik<sup>1,4</sup> , A Koblischka-Veneva<sup>1</sup> ,  
D Gokhfeld<sup>2</sup>  and M Murakami<sup>1</sup>

<sup>1</sup> Superconducting Materials Laboratory, Department of Materials Science and Engineering, Shibaura Institute of Technology, Tokyo 135-8548, Japan

<sup>2</sup> Kirensky Institute of Physics, Federal Research Center KSC SB RAS, Krasnoyarsk, 660036 Russia

E-mail: [miko@shibaura-it.ac.jp](mailto:miko@shibaura-it.ac.jp)

Received 30 September 2019, revised 19 December 2019

Accepted for publication 4 February 2020

Published 19 February 2020



CrossMark

## Abstract

The time-dependence of the field distribution on the surface of  $\text{YBa}_2\text{Cu}_3\text{O}_x$  (YBCO) foam samples after field trapping is analysed. The foam samples were magnetised using a bulk permanent magnet at 77 K, and the trapped fields (TFs) were recorded with a scanning Hall probe 1 mm above the sample surface. Besides a large TF peak, several small peaks are observed. The time dependence of the local fields of these peaks and of the large peak are clearly different, which points to a different origin. In this way, the time-dependent TF measurements reveal important information about the current flow in the foam samples. A non-logarithmic relaxation process takes place in the foam samples. Furthermore, we compare these results with classic creep measurements performed on an individual foam strut removed from the bulk. The creep rate for the TF distribution is found to be  $\sim 8\%$ , whereas the creep rate of the foam strut is about 4% in a large temperature and field range (20–60 K, 0–2 T).

Keywords: YBCO, superconducting foam, trapped fields, flux creep

(Some figures may appear in colour only in the online journal)

## 1. Introduction

Superconducting  $\text{YBa}_2\text{Cu}_3\text{O}_x$  (YBCO) foams exhibit several advantages over common bulk samples, such as the reduced sample weight, the scalability, the short oxygenation time required, the optimum cooling behaviour and the mechanical stability, which are important issues for several types of applications [1–4]. The superconducting foams may have use as bulk trapped field (TF) magnets as proposed in [5, 6], especially in situations where the reduced weight counts, such as in space applications, for example, for flux-pinning docking interfaces in satellites [7]. Even though the present TF values at 77K, achieved using permanent magnets to provide the field, are still relatively small, the situation may change drastically when applying lower temperatures (for example,

50 K) using modern cryocoolers [8] and magnetic fields provided by electromagnets.

Previous magnetisation measurements [9, 10] have shown that foam struts exhibit very high irreversibility fields,  $H_{\text{irr}}$ , being larger than 7T already at  $T = 77$  K. The reason for this behaviour was found in the specific microstructure of the foam struts, which has already been characterised using SEM, electron backscatter diffraction (EBSD) and atomic force microscopy in previous experiments [6, 11]. It was found that the microstructure observed on various foam struts shares certain features with bulk infiltration-growth (IG)-processed samples, but also has a distinct, unique character as the very tiny (20–50 nm diameter)  $\text{Y}_2\text{BaCuO}_5$  (211) particles are arranged in a stripe-like fashion. However, the information concerning the flux creep properties of such samples is still missing, which can provide more details about flux pinning. Thus, this motivated the present investigation on the flux creep effects of superconducting foams.

TF measurements are currently the only non-destructive way to analyse the superconducting properties of large, bulk

<sup>3</sup> Author to whom any correspondence should be addressed.

<sup>4</sup> Current address: Superconducting Electronics Group, Electronics and Photonics Research Institute, National Institute of Advanced Industrial Science and Technology (AIST) 1-1-1 Central 2, Umezono, Tsukuba, Ibaraki, 305-8568, Japan.

superconductors, so we also applied this method to the YBCO foams. The obtained TFs are of the order of 40 mT when magnetizing the samples at 77 K using a large Nd–Fe–B permanent magnet. These TF values are not spectacular as compared with conventional bulk samples [12–15], but at 77 K the bulk samples also do not show TF values higher than 300–400 mT when being magnetized with a permanent magnet. Here, it is important to note that neither the sample size nor the magnetization process were properly optimized to achieve higher TF values. Nevertheless, the TF data obtained on the various sides of the foam sample yield important information on field trapping and the linked current flow within the sample. This provides valuable input for modelling the superconducting properties of a foam sample, required for the design of possible applications. Such modelling may make use of already existing modelling attempts of metallic foams [16, 17], but requires detailed input of the local variation of the superconducting properties of the foam samples.

Another issue for the TF measurements is the waiting time applied between magnetising and measuring the TF data. The flux creep behaviour, which is also present in the classical bulk samples, normally demands a waiting time of about 10–15 min before starting a Hall probe scan [18]. The different microstructure of the foam samples may have an influence on the flux creep behaviour, so the time dependence of the local induction,  $B_{i,z}$ , was measured as a function of time. The possibility to obtain spatially-resolved flux creep data enables us to analyse the flux creep behaviour of different features obtained in the  $B_{i,z}(x, y)$ -data of the foam sample. The analysis of the time-dependence of the  $B_{i,z}(x, y)$ -data obtained was performed using the approach presented in [19], where the flux creep behaviour of the local fields in the superconducting samples was measured using magneto-optic imaging.

Finally, the present experiments enable a direct comparison of the obtained  $TF(t)$ -data on two sides (3), (4) of the bulk foam sample with the flux creep data obtained using SQUID magnetometry on an individual foam strut, which was broken out from the bulk sample. In this way, it is possible to study the time-dependence of the various contributions to the overall current flow in a superconducting foam sample.

## 2. Experimental procedures

### 2.1. Sample preparation and surfaces selected

Open-cell superconducting foams were produced originally at RWTH Aachen (Germany) on the base of polyurethane foams, which were converted in a first step to 211 foams by coating them with a 211 slurry followed by sintering. Then the 211 foams were converted to YBCO using an IG-process—see the review in [20]. More details of the preparation of the foam samples can be found in [1, 2, 21, 22]. In this investigation, a YBCO foam of dimensions  $5 \times 2 \times 2 \text{ cm}^3$  with a porosity of 40 PPI (pores per inch) was employed. The sample investigated is the same one as shown in [6], stemming from RWTH Aachen. Figure 1 presents the selected

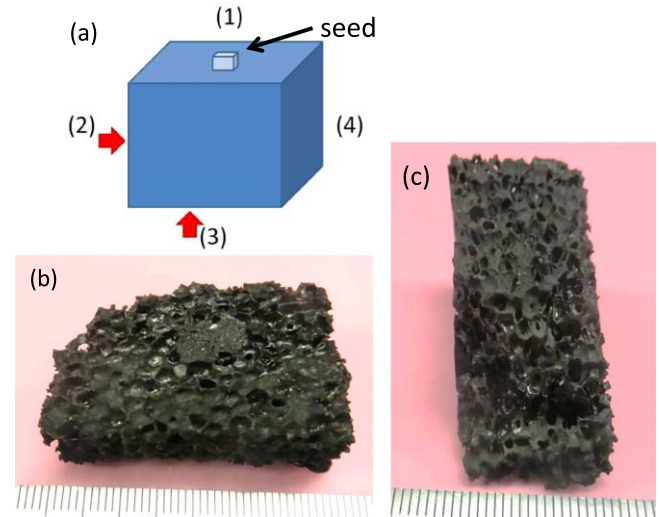


**Figure 1.** (a)–(c) Schematic sketch of the foam sample defining the various sample sides (a) and photographs of the investigated foam sides. (b) The bottom of the foam sample (3), and (c) the right side of the foam, labelled (4). Note some remaining parts of the liquid phase at the bottom of the sample (b).

sample sides (4, foam side) and (3, foam bottom), together with a schematic drawing to explain the naming of the sample sides. Single foam struts were broken off mechanically from the big foam sample for comparison measurements, yielding a sample size of  $\sim 1.4 \times 1.2 \times 0.1 \text{ mm}^3$ . The magnetization hysteresis loops of the foam struts taken from various locations in a bulk foam sample have already been presented in [10].

### 2.2. Magnetic measurements

TF measurements of the large foam piece were carried out using a homemade set-up with a scanning Hall probe operating at 77 K. The foam sample was field cooled (FC) in a field of a commercial, Nd–Fe–B permanent magnet (dimensions of  $60 \times 30 \times 15 \text{ mm}^3$ ) in a liquid nitrogen bath. The TF values were recorded using a Hall probe (size of the active element  $100 \times 100 \mu\text{m}^2$ , sensitivity  $>5 \text{ mV/T}$ ) connected to a Gauss meter (MAGNA model MG-601). The step size in  $x, y$ -directions is 1 mm. A view of this setup is presented in figure 2(a), together with the field distribution produced by the permanent magnet (b). For each measurement in this paper, the permanent magnet was placed above the side analyzed. TF flux density profiles were recorded after 15 min waiting time at 1.5–2 mm height above the foam surface as the surface of the foam was not fully flat, and no surface treatment was carried out. Therefore, the obtained TF values are slightly smaller than that of the other melt-textured bulk samples, which were measured at a distance of 1 mm. Critical current densities were obtained from the TF data with an approximation of Chen's formula [23].

For the time-dependent recording of the flux profiles, the measurements of  $B_{i,z}(x, y)$  have to be repeated several times. Each time stems from a separate experimental run. This

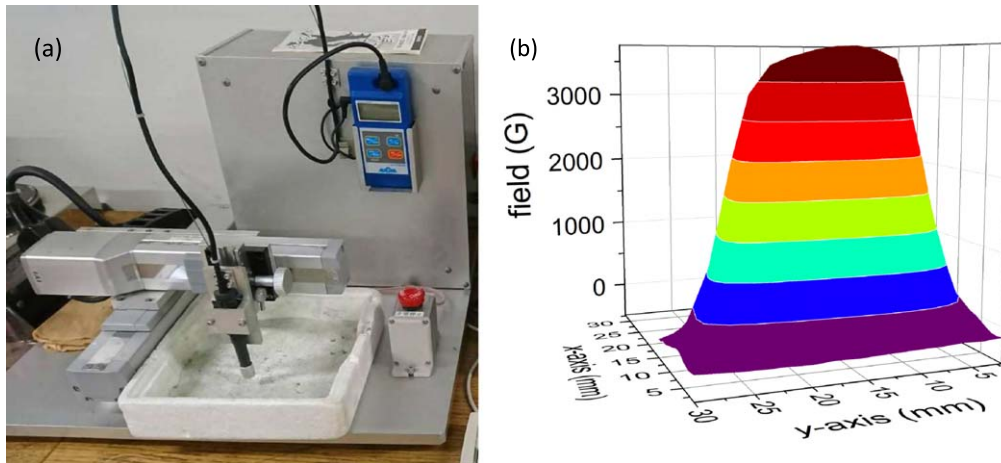


**Figure 2.** (a) The  $x,y$ -positioning measurement set-up equipped with a Hall probe, and (b) the field distribution of the permanent magnet (Nd-Fe-B) employed for the magnetization of the foam sample.

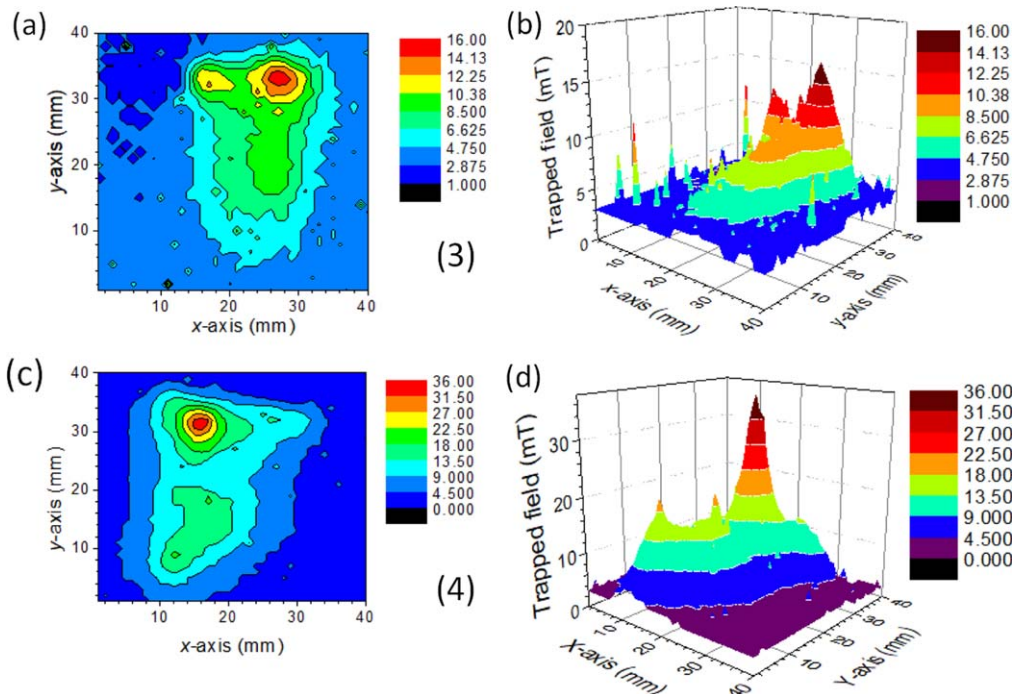


**Figure 3.** (a)–(d) TF distributions,  $B_{i,z}(x, y)$ , for the foam sides (3) and (4) as contour plots (a, c) and 3D-graphs (b, d). The field distributions were recorded after a waiting time of 15 min.

requires a good reproducibility of the starting point of the measurement. The experimental sequence is as follows:

- (i) The foam sample is placed beneath the magnet and left for some time in order to penetrate the flux.
- (ii) Then, the entire assembly is cooled with LN<sub>2</sub>, and kept for some time to ensure that the entire assembly is cooled down properly.
- (iii) In the meantime, the LN<sub>2</sub> container of the  $(x,y)$ -measurement set-up is properly filled with LN<sub>2</sub>. We always take care that the sample is completely immersed in LN<sub>2</sub> to maintain the temperature. Before bringing the FC sample to the measurement system, the bowl is again refilled with LN<sub>2</sub>.

- (iv) After the desired FC time, the sample is quickly moved to the measurement system and the TF profile scan is started.

Measurements were taken at four different times: 5 min, 8 min, 12 min and 15 min. All experiments were repeated at least twice; for  $t = 5$  min and 15 min, three runs were performed in order to check the reproducibility and accuracy. These experimental problems are also a reason why such experiments have not often been performed in the literature—the time-dependence of the local fields are very often investigated only via simulations [24–28].

Magnetisation data of the foam struts in the temperature range  $5 \text{ K} \leq T \leq 86 \text{ K}$  were collected using a SQUID

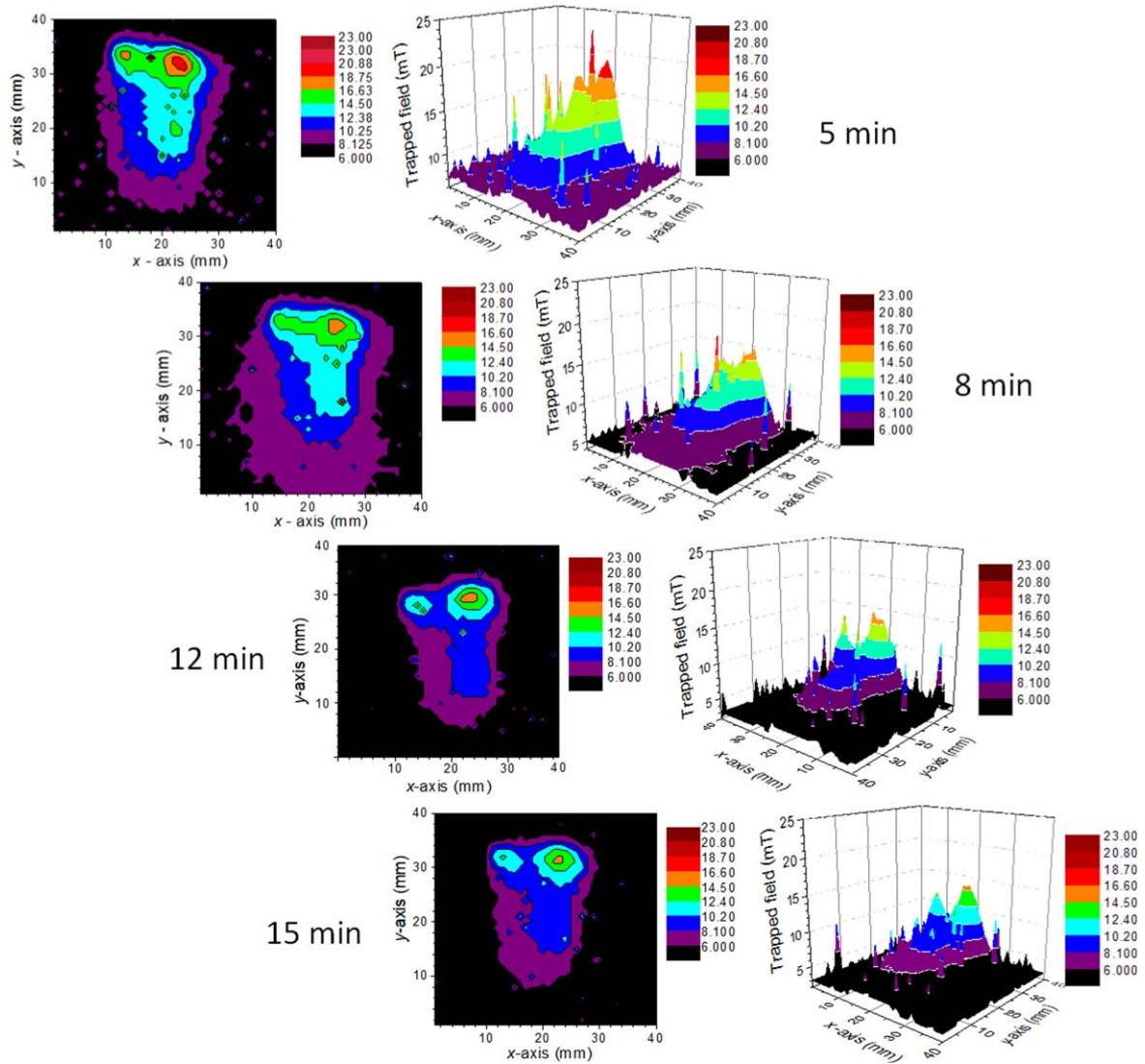


**Figure 4.** (a)–(d) Time-evolution of the TF distribution measured at  $t = 5$  min, 8 min, 12 min and 15 min (from top to bottom) waiting time on the foam side (4).

magnetometer (Quantum Design MPMS3) with  $\pm 7$  T magnetic field applied perpendicular to the foam strut surface. In order to avoid field inhomogeneities, the scan length is set to be 15 mm. The induced current densities are calculated using the extended Bean model [29]. The magnetic relaxation rate is obtained by measuring the time decay of the magnetic moment for 1 h with the magnet in persistent mode. The first data-point was taken after  $t = 200$  s to avoid deviations from pure logarithmic decay.

### 2.3. Flux creep analysis

To analyse the time-dependence of the field profiles, we employ the total flux  $\Phi = B * A$  as a measure ( $B$  denotes the local field and  $A$  is the investigated area), and accordingly, the flux creep rate,  $S$ , is defined as

$$S = \frac{d\Phi(t)}{d(\ln t)}. \quad (1)$$

For the time evolution of the total flux in the sample, we obtain according to [30, 31]

$$\Phi(t, T) = \Phi_0 f(T) \left[ 1 \pm \frac{k_B T}{\langle E(T) \rangle} \ln \left( \frac{t}{1 + t/\tau_0} \right) \right]. \quad (2)$$

Here,  $\Phi_0 = \Phi(t = 0)$  is the starting point of the experiment,  $f(T)$  is a temperature-dependent function,  $k_B$  is the Boltzmann constant,  $\langle E(T) \rangle$  denotes an effective activation energy and  $\tau_0$  represents a characteristic relaxation time. This equation is valid for a chosen region as well as for an overview measurement of the entire sample. To obtain the creep rate,  $S$ , from the data collected, we employ the relation

$$S = \frac{d\Phi(t)}{\Phi_0 d(\ln t)} \Big|_{t=t_{\text{start}}} = - \frac{1}{(\langle E(T) \rangle / k_B T) - \ln(t_{\text{start}}/\tau_0)}, \quad (3)$$

where  $t_{\text{start}}$  is the starting point of the observation. The parameter  $\tau_0$  is of the order of  $10^{-12} \text{ s} \leq \tau_0 \leq 10^{-6} \text{ s}$  for

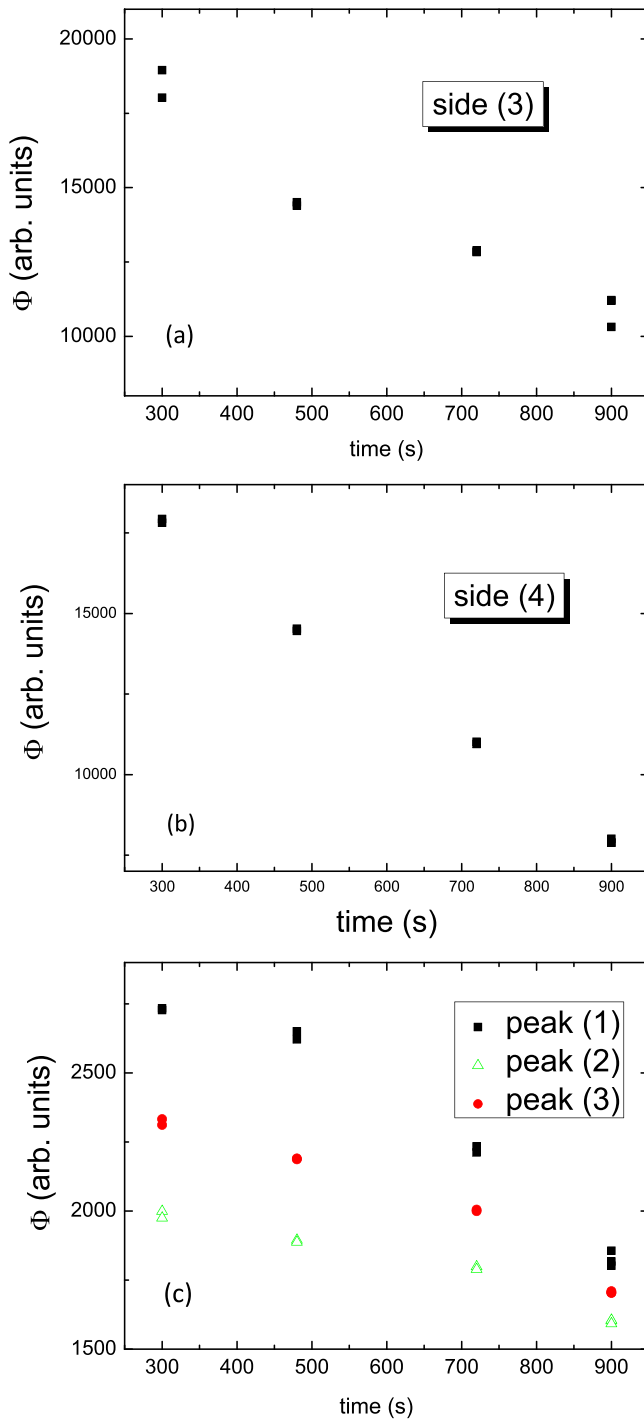


**Figure 5.** Time dependence of the full grid measured ( $40 \times 40$  points) on (a) sample side (3) and (b) sample side (4). Selected small areas ( $3 \times 3$  points) around the sharp peaks are presented in (c).

high- $T_c$  materials [31]. The locally measured data (local induction  $B_i$  or intensity) are then summed up yielding a measure for  $\Phi$ , and the resulting data are plotted in a normalized way ( $\Phi/\Phi_0$ ) to give the creep rate,  $S$ .

This procedure was successfully employed to analyse magneto-optic flux creep data [19, 32]. As the Hall probes measure only the  $z$ -component of  $B_i$ , the present case of a bulk foam sample is better suited for this analysis than the

thin single crystals analysed in [19, 32]. A possible reconstruction of the current flow via inversion of the Biot–Savart law [33] assumes a homogeneous sample with a regular current flow, which is certainly not the case for the present foam samples, so we decided to stay with the analysis of the total flux,  $\Phi$ .

### 3. Results and discussion

#### 3.1. Time-dependence of the TF distribution of bulk foam samples

Firstly, we have a look at the field distributions obtained on the foam sample sides (3) and (4), presented in figure 3(a)–(d) as 3D plots and contour plots. Foam sample side (4) was found in [6] to exhibit the best TF properties. As already noticed in previous publications [6, 34, 35], the foam sample exhibits a large TF peak, but also several sharp, small peaks. The presence of these peaks is characteristic for the foam samples, and is not seen in conventional, melt-textured bulk samples. These peaks with a specific flux distribution give important information regarding the currents flowing in the foam sample: the broad peak is due to currents running through the entire sample perimeter, such as in the case of conventional bulk samples. Of course, these currents are influenced by the presence of pores and are confined to flow within the foam struts. This also implies that these currents are not flowing solely in  $(a,b)$ -planes like in a conventional sample, but face the various orientations of the 3D structure of the foam struts, which can vary by  $\pm 30^\circ$  as revealed by EBSD analysis [11]. The sharp, small peaks are caused by current loops which encircle some pores on well-superconducting current paths, and are compressed due to the currents circulating through the entire sample. Also, these currents have to follow the 3D orientation of the respective foam struts. Here, it is important to note that the foam struts are building up a true 3D structure, and the orientation of the foam struts to the external magnetic field varies considerably. Both types of currents are percolative using all possible superconducting paths in the sample. Therefore, the recorded TFs of these small, sharp peaks may be different and at diverse locations due to the differences in the local microstructure when repeating the experiments. Furthermore, the resulting TF fields can vary when repeating the experiments, as seen in the present investigation.

Now, we look at the time dependence of the TF distribution on side (3) of the foam sample. Figure 4 shows the TF field distribution after a waiting time of (a) 5 min, (b) 8 min, (c) 12 min and, finally, (d) 15 min as contour plots (left) and as 3D-plots (right). From these plots we see that the big TF cone is clearly affected by the flux creep process. The peak value decreases from  $\sim 20$  mT to about 16 mT after 15 min waiting time, which corresponds to a reduction of 20%. Consequently, the currents flowing in the sample are redistributing. Also, the sharp, tiny peaks shrink with time, but the time characteristics are different, which points again to

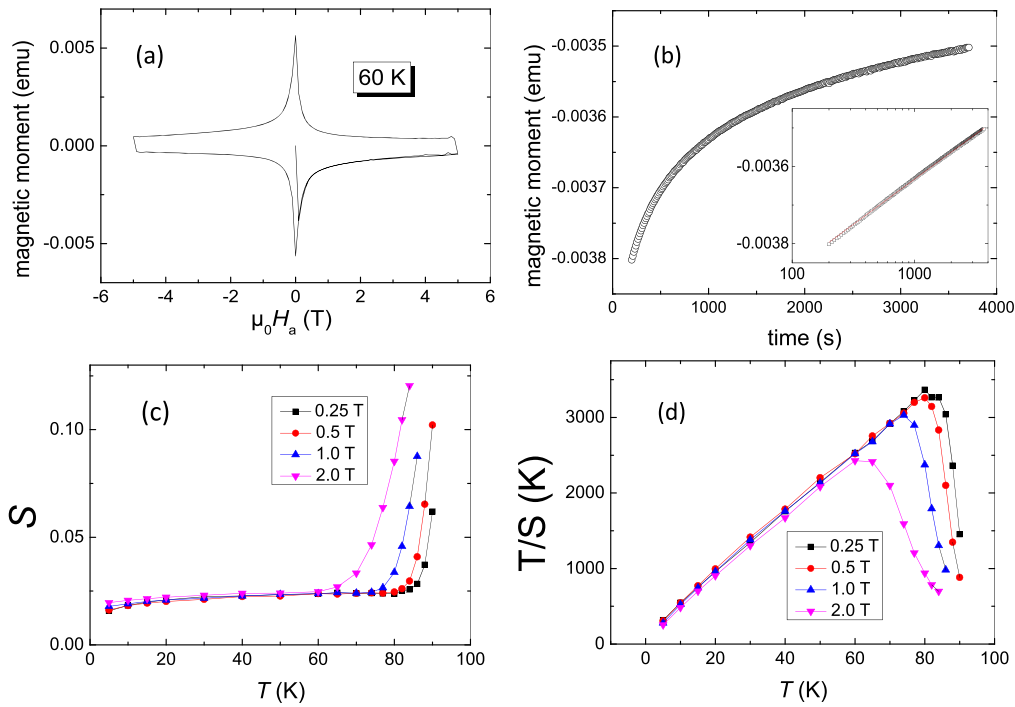


**Figure 6.** Flux creep data obtained on an individual foam strut piece, recorded by SQUID magnetometry. (a) The magnetisation loops of the foam strut taken at  $T = 60$  K, (b) the time evolution of the magnetisation at  $T = 60$  K for a field of  $0.5$  T. The inset shows the logarithmic behaviour of  $S$  and a linear fit to the data (red line). (c)  $S$  as a function of  $T$  for various applied magnetic fields, and (d)  $T/S$  versus  $T$  for various applied magnetic fields.

the different origin. This will be investigated by the time-dependence of the total flux in figure 5 below.

Figures 5(a), (b) present the time-dependence of the total flux  $\Phi$  for the full  $40 \times 40$ -grids measured on sample sides (3) and (4). All data points were repeated at least twice. The time decay of the total local field is obvious, and at first glance, the resulting behaviour looks quite linear. Fitting a linear function to  $\ln(\Phi)$  yields a creep rate  $S = \sim 8\%$ . The relaxation of the sharp peaks was evaluated using a  $3 \times 3$  grid, which has the advantage that the central point of the grid can be placed on the maximum of the peak to account for possible shifts. In this way, we can properly analyse the time-dependent decay of the flux on the specific peak. The results of this procedure are shown in figure 5(c). Here, we clearly see a non-linear behaviour, as the time decay is at first slow, but then considerably increases. This observation is valid for all the sharp, small peaks found in the foam sample. An explanation for this behaviour is as follows: firstly, the compression of the current loops remains unchanged, and only a small relaxation takes place. When the currents flowing through the entire sample perimeter are rearranged, the compression on these small loops releases, and then these current loops are allowed to relax. Thus, there is a characteristic time which indicates the release of the current loop compression. All this causes a non-logarithmic relaxation process, as seen in figure 5(c). Overall, the analysis of the total flux,  $\Phi$ , reveals a strong relaxation of the TFs, reaching a maximum of about 20% in the case of the peak value of the large peak. Other regions of the TF distribution show a much smaller relaxation, so an overall flux creep rate of

approximately 8% results from our analysis for all TF distributions studied here.

The present flux creep data reveal that a 15 min waiting time before starting the Hall probe scan is also justified for the bulk foam samples.

### 3.2. Flux creep analysis of a single foam strut

For comparison with the bulk sample data, we examine here the flux creep behaviour measured by SQUID magnetometry on an individual foam strut. In such a strut, the current flow is limited to the circumference of this strut, so the percolative current flow through the bulk sample caused by the presence of the pores is eliminated here.

Figures 6(a)–(d) present the flux creep data on a broken-out foam strut. Figure 6(a) gives a magnetisation loop of the foam strut at  $T = 60$  K. In figure 6(b), the typical time-decay of the  $M(T, t)$  signal is shown for  $T = 60$  K and an applied magnetic field of  $0.5$  T. The inset shows the logarithmic plot of the magnetisation versus time, together with a linear fit to the data. All flux creep data recorded show a well-developed logarithmic behaviour, except at the highest temperatures measured ( $86$  K). The resulting data for  $S$  at various temperatures and magnetic fields are presented in figure 6(c), and figure 6(d) shows the relation of  $T/S$  versus  $T$  for various applied fields. A typical creep rate of 4% is observed, which is similar or even lower than those seen in melt-textured NdBCO [36] or in YBCO films [37]. As the magnetisation loops of the foam struts do not exhibit a fishtail shape, the resulting  $S(T, B)$  curves are dominantly

flat in a large field region. These flux creep data of the foam strut piece directly reveals the strong flux pinning contribution of the tiny Y-211 particles which were found in electron backscatter diffraction analysis [6, 11, 38]. Furthermore, it must be remarked here that the field is not oriented parallel to the  $c$ -axis of the material, but about  $30^\circ$  off. The YBCO matrix of the foam strut is also not completely homogeneous but consists of several well-aligned YBCO grains, as observed in our previous EBSD investigations [6, 11, 38]. Thus, even though the currents within a foam strut may face several grain boundaries, the overall current strength is very high due to the improved flux pinning properties provided by the tiny 211 particles embedded within the YBCO matrix, which is common for all IG-processed YBCO superconductors.

The well-developed flux-pinning properties within the individual foam struts give rise to the hope that the overall TF behaviour of the foam samples will considerably improve when moving towards lower temperatures such as 77 K, for example, 50 K could be an interesting target temperature located right on the plateau of  $S(T)$ , as seen in figure 6(c). Then, also the critical currents will be much stronger, thus we may expect to measure much larger TFs in the foam samples.

#### 4. Conclusions

The flux creep behaviour of bulk foam samples is investigated using time-dependent TF measurements. From these data, we obtain important information on the current flow in a bulk foam sample as the time-dependence of the broad peak and that of the small, sharp peak is distinctly different, pointing to a different origin. An overall flux creep rate of  $\sim 8\%$  is obtained from our analysis of the time-dependent TF data, so these data demonstrate that a waiting time of 15 min before starting the Hall probe measurement is also required for the bulk foam samples. The flux creep analysis performed on an individual foam strut piece reveals relatively strong flux pinning as the flux creep rates obtained from SQUID magnetometry (typical value of  $S = 4\%$ ) are similar or even lower than those of the melt-textured NdBCO samples or even the YBCO thin film samples.

#### Acknowledgments

We thank G Schmitz (ACCESS, Aachen, Germany) for providing us with the foam sample, and K Berger, B Douine and Q Nouailhetas (GREEN, Nancy, France) for valuable discussions concerning applications of the superconducting foam materials. This work is part of the SUPERFOAM International Project funded by ANR and DFG under references ANR-17-CE05-0030 and DFG-ANR Ko2323-10, respectively.

#### ORCID iDs

M R Koblischka  <https://orcid.org/0000-0003-4924-341X>  
 S Pavan Kumar Naik  <https://orcid.org/0000-0002-9343-4320>  
 A Koblischka-Veneva  <https://orcid.org/0000-0001-7409-671X>  
 D Gokhfeld  <https://orcid.org/0000-0001-9049-9973>

#### References

- [1] Reddy E S and Schmitz G J 2002 Superconducting foams *Supercond. Sci. Technol.* **15** L21–4
- [2] Noudem J G 2011 Developing of shaping textured superconductors *J. Supercond.* **24** 105–10
- [3] Laurent P, Mathieu J-P, Mattivi B, Fagnard J-F, Meslin S, Noudem J G, Ausloos M, Cloots R and Vanderbemden P 2005 Study by Hall probe mapping of the trapped flux modification produced by local heating in YBCO HTS bulks for different surface/volume ratios *Supercond. Sci. Technol.* **18** 1047–53
- [4] Jung A, Diebels S, Koblischka-Veneva A, Schmauch J, Barnoush A and Koblischka M R 2013 Microstructural analysis of electrochemical coated open-cell metal foams by EBSD and nanoindentation *Adv. Eng. Mater.* **16** 15–20
- [5] Koblischka M R and Koblischka-Veneva A 2018 Porous high- $T_c$  superconductors and their applications *AIMS Mater. Sci.* **5** 1199–213
- [6] Koblischka M R, Pavan Kumar Naik S, Koblischka-Veneva A, Murakami M, Gokhfeld D, Reddy E S and Schmitz G J 2019 Superconducting YBCO foams as trapped field magnets *Materials* **12** 853
- [7] Shoer J, Wilson W, Jones L, Knobel M and Peck M 2010 Microgravity demonstrations of flux pinning for station-keeping and reconfiguration of cubesat-sized spacecraft *J. Spacecr. Rockets* **47** 1066–9
- [8] Radebaugh R 2009 Cryocoolers: the state of the art and recent developments *J. Phys. C* **21** 164219
- [9] Koblischka M R, Koblischka-Veneva A, Chang C, Hauet T, Reddy E S and Schmitz G J 2019 Flux pinning analysis of superconducting YBCO foam struts *IEEE Trans. Appl. Supercond.* **29** 8001905
- [10] Koblischka M R, Koblischka-Veneva A, Berger K, Nouailhetas Q, Douine B, Reddy E S and Schmitz G J 2019 Current flow and flux pinning properties of YBCO foam struts *IEEE Trans. Appl. Supercond.* **29** 8001405
- [11] Koblischka M R, Koblischka-Veneva A, Reddy E S and Schmitz G J 2014 Analysis of the microstructure of superconducting YBCO foams by means of AFM and EBSD *J. Adv. Ceram.* **3** 317–25
- [12] Wang Y-N, Yang W-M, Yang P-T, Zhang C-Y, Chen J-L, Zhang L-J and Chen L 2017 Influence of trapped field on the levitation force of SmBCO bulk superconductor *Physica C* **542** 28–33
- [13] Zhou D A, Shi Y, Zhao W, Dennis A R, Beck M, Ainslie M D, Palmer K G B, Cardwell D A and Durrell J H 2017 Full magnetization of bulk (RE)Ba<sub>2</sub>Cu<sub>3</sub>O<sub>7- $\delta$</sub>  magnets with various rare-earth elements using pulsed fields at 77 K *IEEE Trans. Appl. Supercond.* **27** 6800704
- [14] Hari Babu N, Kambara M, Smith P J, Cardwell D A and Shi Y 2000 Fabrication of large single-grain Y–Ba–Cu–O through infiltration and seeded growth processing *J. Mater. Res.* **15** 1235–8
- [15] Liu Y, Pan B, Li Z, Xiang H, Qian J, Du G, Huang S, Yao X, Izumi M and Wang Y 2017 YBa<sub>2</sub>Cu<sub>3</sub>O<sub>7- $\delta$</sub>  superconductor

- bulks composited by  $\text{Y}_2\text{BaCuO}_5$  nanoparticles derived from homogeneous nucleation catastrophe *J. Am. Ceram. Soc.* **100** 3858–64
- [16] Montminy M D, Tannenbaum A R and Macosko C W 2004 The 3D structure of real polymer foams *J. Colloid Interface Sci.* **280** 202–11
- [17] Nie Z, Lin Y and Tong Q 2017 Modeling structures of open cell foams *Comput. Mater. Sci.* **131** 160–9
- [18] Cardwell D A *et al* 2004 Round robin measurements of the flux trapping properties of melt processed Sm-Ba-Cu-O bulk superconductors *Physica C* **412–414** 623–32
- [19] Koblischka M R, Schuster T, Ludescher B and Kronmüller H 1992 Direct observation of flux-creep in high- $T_c$  superconductors using the high-resolution Faraday effect *Physica C* **190** 557–62
- [20] Devendra Kumar N, Shi Y-H and Cardwell D A 2016 Fabrication of bulk (RE)BCO superconductors by the infiltration and growth process: past, present and future *Superconductivity Applications Today and Tomorrow* ed M Muralidhar (New York: NOVA Science Publishers) ch 1, pp 1–35
- [21] Reddy E S and Schmitz G J 2002 Ceramic foams *Am. Ceram. Soc. Bull.* **81** 35–7
- [22] Reddy E S, Herweg M and Schmitz G J 2003 Processing of  $\text{Y}_2\text{BaCuO}_5$  foams *Supercond. Sci. Technol.* **16** 608–12
- [23] Chen I-G, Liu J, Weinstein R and Lau K 1992 Characterization of  $\text{YBa}_2\text{Cu}_3\text{O}_7$ , including critical current density  $J_c$ , by trapped magnetic field *J. Appl. Phys.* **72** 1013–20
- [24] Deng Z, Tsuzuki K, Miki M, Felder B, Hara S and Izumi M 2012 Relaxation properties of the trapped flux of bulk high-temperature superconductors at different magnetization levels *J. Supercond. Nov. Magn.* **25** 331–8
- [25] Ainslie M D, Weinstein R and Sawh R-P 2019 An explanation for observed flux creep in opposite direction to Lorentz force in partially magnetized bulk superconductors *IEEE Trans. Appl. Supercond.* **29** 6801004
- [26] Parks D, Weinstein R, Davey K and Sawh R-P 2013 A study of pulsed activation of trapped field magnets—part 1: effects of pulse height and creep *IEEE Trans. Appl. Supercond.* **23** 6800305
- [27] Selva K, Li X F and Majkic G 2015 Trapped field and flux creep in stacked  $(\text{Gd,Y})\text{Ba}_2\text{Cu}_3\text{O}_x$  superconductor tape arrays *IEEE Trans. Appl. Supercond.* **25** 6605005
- [28] Trillaud F, Berger K, Douine B and Lévêque J 2016 Comparison between modeling and experimental results of magnetic flux trapped in YBCO bulks *IEEE Trans. Appl. Supercond.* **26** 6800305
- [29] Wiesinger H P, Sauerzopf F M and Weber H W 1992 On the calculation of  $j_c$  from magnetization measurements on superconductors *Physica C* **203** 121–8
- [30] Hagen C W and Griessen R P 1989 Distribution of activation energies for thermally activated flux motion in high- $T_c$  superconductors: an inversion scheme *Phys. Rev. Lett.* **62** 2857–61
- [31] Yeshurun J, Malozemoff A P and Shaulov A 1996 Magnetic relaxation in high-temperature superconductors *Rev. Mod. Phys.* **68** 911–49
- [32] Schuster T, Koblischka M R, Kuhn H, Kronmüller H, Leghissa M, Gerhäuser W, Saemann-Ischenko G, Neumüller H W and Klaumünzer S 1992 Observation of flux penetration in BSCCO crystals with irradiation-induced columnar defects *Phys. Rev. B* **46** 8496–504
- [33] Pashitski A E, Gurevich A, Polyanskii A A, Larbalestier D C, Goyal A, Specht E D, Kroeger D M, DeLuca J A and Tkaczyk J E 1997 Reconstruction of current flow and imaging of current-limiting defects in polycrystalline superconducting films *Science* **275** 367–9
- [34] Bartolomé E, Granados X, Puig T, Obradors X, Reddy E S and Schmitz G J 2004 Critical state in superconducting single-crystalline  $\text{YBa}_2\text{Cu}_3\text{O}_7$  foams: local versus long-range currents *Phys. Rev. B* **70** 144514
- [35] Carrera M, Amoros J, Carrillo A E, Obradors X and Fontcuberta J 2003 Current distribution maps in large YBCO melt-textured blocks *Physica C* **385** 539–43
- [36] van Dalen A J J, Koblischka M R, Kojo H, Sawada K, Higuchi T and Murakami M 1996 Low magnetic relaxation in a single crystal and a melt processed  $\text{NdBa}_2\text{Cu}_3\text{O}_{7-\delta}$  sample *Supercond. Sci. Technol.* **9** 659–64
- [37] van Dalen A J J, Griessen R, Libbrecht S, Osquiguil E and Bruynseraede Y 1994 Observation of quantum creep in oxygen deficient  $\text{YBa}_2\text{Cu}_3\text{O}_{7-\delta}$  at fields up to 7 T *Physica C* **235–240** 2959–60
- [38] Koblischka-Veneva A, Koblischka M R, Ide N, Inoue K, Muralidhar M, Hauet T and Murakami M 2016 Microstructural and magnetic analysis of a superconducting foam and comparison with IG-processed bulk samples *J. Phys. Conf. Ser.* **695** 012002